AGU PUBLICATIONS

Geophysical Research Letters

Supporting Information for

Anthropogenic Aerosols Significantly Reduce Mesoscale Convective System Occurrences and Precipitation over Southern China in April

Lijuan Zhang[1], Tzung-May Fu[2,3,*], Heng Tian[1], Yaping Ma[1], Jen-ping Chen[4,5], Tzu-Chin Tsai[4], I-Chun Tsai[6], Zhiyong Meng[1], Xin Yang[2,3]

[1] Department of Atmospheric and Oceanic Sciences, School of Physics, Peking University, China

[2] School of Environmental Science and Engineering, Southern University of Science and Technology, Shenzhen, Guangdong Province, China

[3] Shenzhen Institute of Sustainable Development, Southern University of Science and Technology, Shenzhen, Guangdong Province, China

[4] Department of Atmospheric Sciences, National Taiwan University, Taiwan

[5] International Degree Program in Climate Change and Sustainable Development, National Taiwan University, Taiwan

[6] Research Center for Environmental Changes, Academia Sinica, Taiwan

* Corresponding author: Tzung-May Fu (fuzm@sustech.edu.cn)

Contents of this file

Introduction

- Text S1 describes the model, the emission inventories, the experimental design, and the validation of model results
- Text S2 describes the objective diagnosis of MCS occurrences.
- Text S3 describes of the composite normalized contoured frequency by altitude diagram.
- Descriptions of Figures S1-S8 and Tables S1-S3 are shown in the corresponding figure and table caption.

Text S1.

WRF-Chem model configuration, emission inventories, experimental design, and model validation

Simulations with the Weather Research and Forecasting Model coupled to Chemistry (WRF-Chem, v3.6.1) [*Grell et al.*, 2005] were performed using three nested domains (Figure S2), with horizontal resolutions of 27 km, 9 km, and 3 km, respectively. Initial and boundary conditions for meteorological variables were from the NCEP FNL Operational Global Analysis data (https://rda.ucar.edu/datasets) and updated every 6 hours. To maintain stability of the model for longer simulations, meteorological fields above 2.6 km (level 10) in the outer-most domain was nudged toward the NCEP FNL data every 5 days. Initial and boundary concentrations of chemical species in the outer-most domain were from a global simulation using the MOZART-4 model [*Emmons et al.*, 2010] and updated every 6 hours. All simulations were conducted from March 25 to May 1 of the corresponding year. The first 7 days spun up the simulations. Results from the inner-most domain between April 1 and May 1 were analyzed.

We configured the WRF-Chem model to simulate the direct and indirect radiative effects of aerosols. Aerosol microphysics were simulated with the MADE/SORGAM scheme [*Ackermann et al.*, 1998; *Schell et al.*, 2001]. Cloud microphysics was simulated using a double-moment bulk microphysics scheme [*Morrison et al.*, 2005, 2009], which calculates the mixing ratios and the number concentrations of five hydrometeors: cloud droplets, rain drops, ice crystals, snow, and graupel. The activation of CCN was simulated using the κ-Köhler theory [*Petters and Kreidenweis*, 2007], which accounted for the different hygroscopicity of different aerosol species. The standard Morrison scheme in WRF-Chem considers the impacts of aerosols on CCN activation, but the IN-activation is independent of aerosol number. We modified the IN-activation scheme in WRF-Chem, such that the number of activated IN was dependent on temperature and the number concentrations of particles larger than 0.5 μm in diameter [*DeMott et al.*, 2010]. Radiative scattering and absorption by aerosol and clouds were simulated using the Goddard shortwave radiation scheme [*Chou and Suarez*, 1994], which explicitly calculated the liquid cloud optical thickness using liquid cloud water content and liquid cloud droplet numbers. Other physical and chemical parameterizations in our WRF-Chem simulations were as summarized in Table S1.

Chinese emissions of aerosols and precursors from anthropogenic sources (including power generation, industry, residential, transportation, and agriculture) were from the Multi-resolution Emission Inventory for China (MEIC) [*Liu et al.*, 2015], developed for the year 2010 at a native resolution of 0.25°. Anthropogenic emissions for the rest of Asia were from *Zhang et al.* [2009], developed for the year 2006 at a native resolution of 0.5°. Biomass burning emissions were taken from the Fire

Inventory from NCAR (FINN) [*Wiedinmyer et al.*, 2011], developed for the year 2009 at 1-km resolution. All emission data were interpolated to model resolutions to drive WRF-Chem. The same anthropogenic and biomass burning emissions were used for both 2009 and 2010 simulations. Biogenic emissions were calculated online in WRF-Chem using the MEGAN algorithm version 2 [*Guenther et al.*, 2006].

All emissions were included in the 'polluted' simulations, while Chinese anthropogenic emissions were excluded in the 'clean' simulations. In the "Polluted_NoADE" simulations, the direct radiative effects of aerosols were turned off. In the "Polluted_0.5LCOT" simulations, we reduced the liquid cloud optical thickness (LCOT) in the inner-most domain by 50% only in the radiative calculations. The microphysical calculations were not manually altered. The effect of reducing the LCOT by 50% in the radiative calculations in our simulation was approximately equivalent to turning off the Twomey effect of aerosols on warm clouds. In the "Polluted_0.5LCOT_NoADE" simulations, the direct radiative effects of aerosols were turned off and the LCOT used in the radiative calculations were reduced by 50% in the inner-most domain. All other model configurations were the same as those in the polluted simulations.

The modeled accumulated rainfall and rainfall intensity over Southern China in the "polluted" simulations compared well with surface rain gauge observations in April

2009 (Figure S4), indicating that the model was able to capture the general regional climate. The average number concentrations of fine aerosols at the surface over Southern China were 3×10^4 cm^{-3} in the polluted simulations and 2×10^3 cm^{-3} in the clean simulations. These numbers are respectively similar to the fine aerosol concentrations observed at urban (1.4×10^4 to 2.6×10^4 cm^{-3}) and background (approximately 2×10^3 cm^{-3}) sites in Southern China [*Huang et al.*, 2017]. The monthly domain-averaged clear-sky aerosol optical depth (AOD) over Southern China in the polluted simulations of April 2009 and April 2010 were 0.54 and 0.61, respectively, comparable to the clear-sky AOD observed by MODIS (https://modis.gsfc.nasa.gov/) of 0.4-0.8. The domain-average monthly mean $PM_{2.5}$ concentrations over Southern China in the polluted simulations of April 2009 and April 2010 were 21.1 μg m^{-3} and 20.7 μg m^{-3}, respectively, comparable to the observed 23.3±4.5 μg m^{-3} over Southern China in April [*Lai et al.* 2016]. In the polluted simulations of both April 2009 and April 2010, the sum of sulfate, nitrate, and ammonium accounted for 30% to 57% of surface $PM_{2.5}$, similar to the 33% to 66% observed in Southern China in April 2009 [*Tao et al.* 2014]. These evidences indicated that the model was able to represent the aerosol and microphysical conditions over Southern China in April.

Text S2.

Objective diagnosis of MCS occurrences

Based on widely-accepted definitions of MCSs [*Parker and Johnson*, 2000], we developed an automated algorithm to objectively identify the occurrence of an MCS as the presence of a strictly contiguous surface area satisfying the following criteria: (1) all surface grids within the area had RADAR reflectivity ≥40 dBZ somewhere in the vertical column of air above it; (2) some model grids within that contiguous area had ≥45 dBZ RADAR reflectivity; (3) the contiguous area extended ≥100 km in at least one horizontal direction (4) but extended ≤250 km in all horizontal directions. The total number-hours of MCS occurrences calculated the sum of hours that each individual MCS was present. MCS rainfall was defined as the precipitation that fell within the MCS area, including both MCS stratiform rainfall and MCS convective rainfall. MCS convective rainfall was defined as the MCS rainfall which fall over grids with RADAR reflectivity ⩾35 dBZ somewhere in the vertical column of air above it.

We found that MCS occurrences were suppressed in the polluted simulations relative to those in the clean simulations (Section 3 in the main text). We further confirmed that this suppression of MCS occurrences by aerosols was not affected by changes in the threshold criteria used in the automated algorithm:

- If we changed the threshold criteria in (1) from ⩾40 dBZ to ⩾35 dBZ: the number-hours of MCS occurrences were 890 hours under clean conditions and 687 hours under polluted conditions for April 2009 (-22% reduction under polluted conditions relative to clean conditions). The number-hours of MCS occurrences were 1214 hours under clean conditions and 1032 hours under polluted conditions for April 2010 (-15% reduction under polluted conditions relative to clean conditions).

- If we changed the threshold criteria in (2) from ⩾45 dBZ to ⩾40 dBZ: the number-hours of MCS occurrences were 742 hours under clean conditions and 509 hours under polluted conditions for April 2009 (-31% reduction under polluted conditions). The number-hours of MCS occurrences were 995 hours under clean conditions and 783 hours under polluted conditions for April 2010 (-21% reduction under polluted conditions).

- If we changed the threshold criteria in (4) from ⩽250 km to ⩽200 km: the number-hours of MCS occurrences were 584 hours under clean conditions and 406 hours under polluted conditions for April 2009 (-30% reduction under polluted conditions). The number-hours of MCS occurrences were 832 hours under clean conditions and 661 hours under polluted conditions for April 2010 (-21% reduction under polluted conditions).

Text S3.

Composite normalized contoured frequency of RADAR reflectivity

We composited the model results of the RADAR reflectivity (Z) for all simulated MCSs to construct the composite normalized contoured frequency by altitude diagram [*Yuter and Houze,* 1995] (CFAD, Figure 3):

$$\mathrm{CFAD}_{ij} = \frac{\int_{H_i}^{H_i+\Delta H}\int_{Z_j}^{Z_j+\Delta Z} \frac{\partial^2 N(H,Z)}{\partial H \partial Z}\, dZdH}{\Delta Z \Delta H \int_{0}^{H_{top}}\int_{-\infty}^{\infty} \frac{\partial^2 N(H,Z)}{\partial H \partial Z}\, dZdH}$$

where $N(H, Z)$ is the frequency distribution function defined as the number of Z in the range of Z to $Z+\Delta Z$ at a height(H) above ground ranging from H to $H+\Delta H$. The index i goes from 1 to 120 in intervals of 0.1 km. The index j goes from -10 to 65 in intervals of 2.5 dBZ.

References:

Ackermann, I. J., H. Hass, M. Memmesheimer, A. Ebel, F. S. Binkowski, and U. Shankar (1998), Modal aerosol dynamics model for Europe: Development and first applications, *Atmos. Environ.*, *32*(17), 2981-2999, doi:10.1016/s1352-2310(98)00006-5.

Chou, M.-D., and M. J. Suarez (1994), *An Efficient Thermal Infrared Radiation Parameterization for Use in General Circulation Models*, NASA Technical Memorandum No. 104606, Vol.3, 85p. https://archive.org/details/nasa_techdoc_19950009331.

DeMott, P. J., A. J. Prenni, X. Liu, S. M. Kreidenweis, M. D. Petters, C. H. Twohy, M. S. Richardson, T. Eidhammer, and D. C. Rogers (2010), Predicting global atmospheric ice nuclei distributions and their impacts on climate, *Proc. Natl. Acad. Sci. USA*, *107*(25), 11217-11222, doi:10.1073/pnas.0910818107.

Emmons, L. K., et al. (2010), Description and evaluation of the Model for Ozone and Related chemical Tracers, version 4 (MOZART-4), *Geosci. Model Dev.*, *3*(1), 43-67, doi:10.5194/gmd-3-43-2010.

Grell, G. A., S. E. Peckham, R. Schmitz, S. A. McKeen, G. Frost, W. C. Skamarock, and B. Eder (2005), Fully coupled "online" chemistry within the WRF model, *Atmos. Environ.*, *39*(37), 6957-6975, doi:10.1016/j.atmosenv.2005.04.027.

Guenther, A., T. Karl, P. Harley, C. Wiedinmyer, P. I. Palmer, and C. Geron (2006), Estimates of global terrestrial isoprene emissions using MEGAN (Model of Emissions of Gases and Aerosols from Nature), *Atmos. Chem. Phys.*, *6*, 3181-3210, doi:10.5194/acp-6-3181-2006.

Huang, X. F., C. Wang, J. F. Peng, L. Y. He, L. M. Cao, Q. Zhu, J. Cui, Z. J. Wu, and M. Hu (2017), Characterization of particle number size distribution and new particle formation in Southern China, J. Environ. Sci., 51, 342-351, doi:10.1016/j.jes.2016.05.039.

Lai, S. C., Y. Zhao, A. J. Ding, Y. Y. Zhang, T. L. Song, J. Y. Zheng, K. F. Ho, S. C. Lee, and L. J. Zhong (2016), Characterization of PM2.5 and the major chemical components during a 1-year campaign in rural Guangzhou, Southern China, *Atmos. Res.*, *167*, 208-215, doi:10.1016/j.atmosres.2015.08.007.

Liu, F., Q. Zhang, D. Tong, B. Zheng, M. Li, H. Huo, and K. B. He (2015), High-resolution inventory of technologies, activities, and emissions of coal-fired power plants in China from 1990 to 2010, *Atmos. Chem. Phys.*, *15*(23), 13299-13317, doi:10.5194/acp-15-13299-2015.

Morrison, H., J. A. Curry, and V. I. Khvorostyanov (2005), A new double-moment microphysics parameterization for application in cloud and climate models. Part I: Description, *J. Atmos. Sci.*, *62*(6), 1665-1677, doi:10.1175/jas3446.1.

Morrison, H., G. Thompson, and V. Tatarskii (2009), Impact of Cloud Microphysics on the Development of Trailing Stratiform Precipitation in a Simulated Squall Line: Comparison of One- and Two-Moment Schemes, *Mon. Weather Rev.*, *137*(3), 991-1007, doi:10.1175/2008mwr2556.1.

Parker, M. D., and R. H. Johnson (2000), Organizational modes of midlatitude mesoscale convective systems, *Mon. Weather Rev.*, *128*(10), 3413-3436, doi:10.1175/1520-0493(2001)129<3413:omommc>2.0.co;2.

Petters, M. D., and S. M. Kreidenweis (2007), A single parameter representation of hygroscopic growth and cloud condensation nucleus activity, *Atmos. Chem. Phys.*, *7*(8), 1961-1971, doi:10.5194/acp-7-1961-2007.

Schell, B., I. J. Ackermann, H. Hass, F. S. Binkowski, and A. Ebel (2001), Modeling the formation of secondary organic aerosol within a comprehensive air quality model system, *J. Geophys. Res. Atmos.*, *106*(D22), 28275-28293, doi:10.1029/2001jd000384.

Tao, J., L. M. Zhang, K. F. Ho, R. J. Zhang, Z. J. Lin, Z. S. Zhang, M. Lin, J. J. Cao, S. X. Liu, and G. H. Wang (2014), Impact of PM2.5 chemical compositions on aerosol light scattering in Guangzhou - the largest megacity in South China, *Atmos. Res.*, *135*, 48-58, doi:10.1016/j.atmosres.2013.08.015

Wiedinmyer, C., S. K. Akagi, R. J. Yokelson, L. K. Emmons, J. A. Al-Saadi, J. J. Orlando, and A. J. Soja (2011), The Fire INventory from NCAR (FINN): a high resolution global model to estimate the emissions from open burning, *Geosci. Model Dev.*, *4*(3), 625-641, doi:10.5194/gmd-4-625-2011.

Yuter, S. E., and R. A. Houze (1995), Three-Dimensional Kinematic and Microphysical Evolution of Florida Cumulonimbus. Part II: Frequency Distributions of Vertical Velocity, Reflectivity, and Differential Refectivity, *Mon. Weather Rev.*, *123*(7), 1941-1963, doi:10.1175/1520-0493(1995)123<1941:tdkame>2.0.co;2.

Zhang, Q., et al. (2009), Asian emissions in 2006 for the NASA INTEX-B mission, *Atmos. Chem. Phys.*, *9*(14), 5131-5153, doi:10.5194/acp-9-5131-2009.

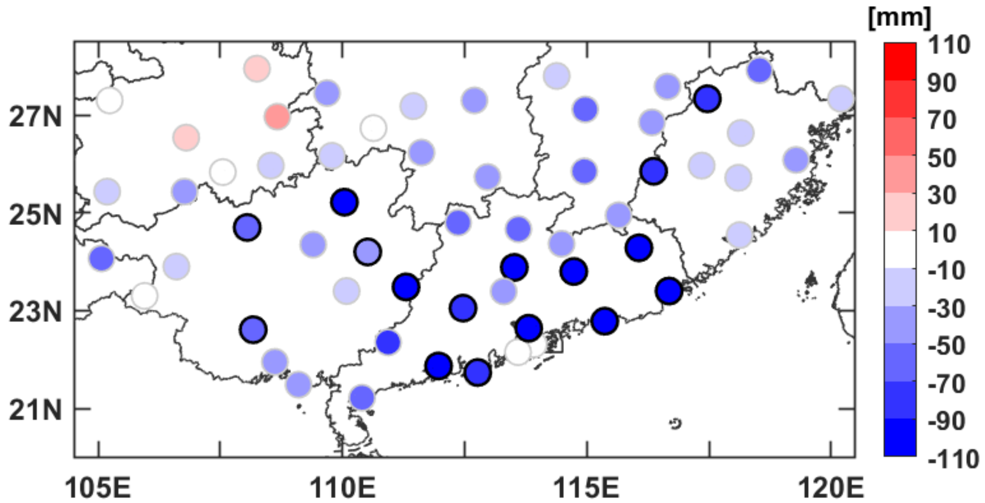

Figure S1. Observed differences in April precipitation at 59 surface meteorological stations over Southern China between the years 2001-2011 versus the years 1979-1989. Red and blue symbols indicate increases and decreases of precipitation, respectively. Symbols with black circles indicate stations where the difference in precipitation was significant at the 90% confidence level.

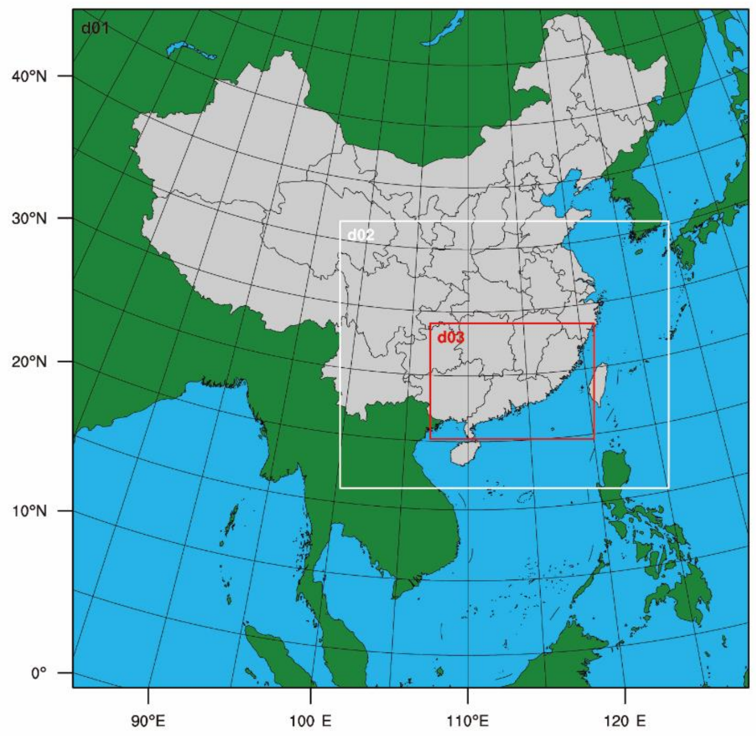

Figure S2. The three nested domains used in our WRF-Chem simulations, with horizontal resolutions of 27 km (d01), 9 km (d02), and 3 km (d03), respectively. The red box indicates the Southern China region. The grey color indicates the Chinese area where anthropogenic emissions were turned off for the ‘clean’ simulations.

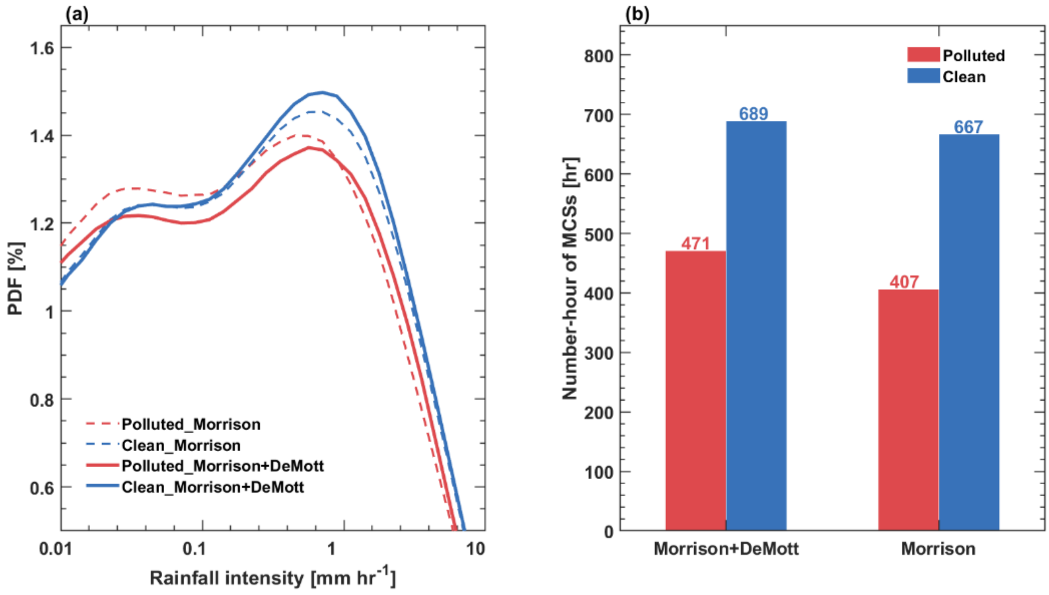

Figure S3. Comparison of the rainfall intensity and MCS occurrences simulated for April 2009 using the standard Morrison scheme (labeled as 'Morrison') against those simulated using the Morrison scheme with the addition of aerosol number-dependent IN-activation (labeled as 'Morrison+DeMott'): (a) probability distribution functions of rainfall intensity in the sensitivity simulations of April 2009; (b) the total number-hours of MCSs over Southern China in April 2009 parsed from the hourly model outputs of the sensitivity simulations. Color codes for the sensitivity simulations are shown inset.

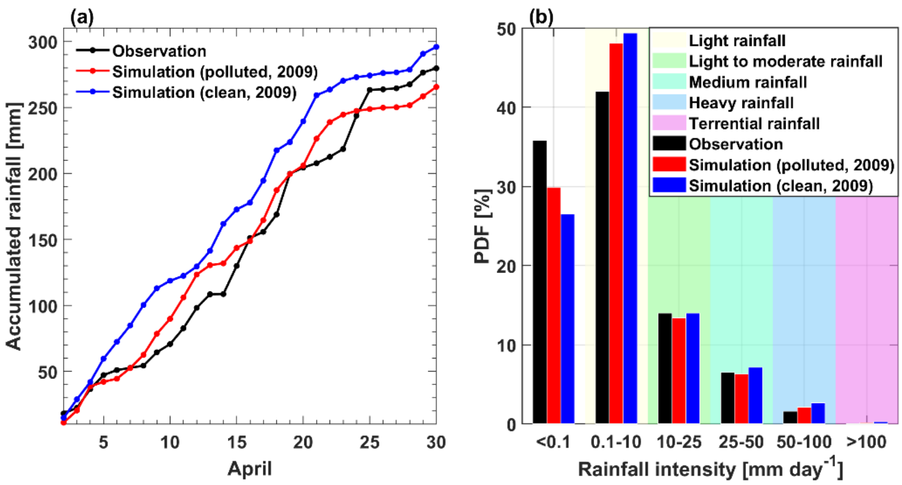

Figure S4. (a) Observed (black) and simulated (polluted, red; clean, blue) accumulated daily rainfall averaged for 59 surface stations (shown in Figure S1) in Southern China for April 2009. (b) Observed (black) and simulated (polluted, red; clean, blue) probability distribution function of daily rainfall intensity at 59 surface stations in Southern China for April 2009. The color codes for categories of rainfall intensities, as defined by the Chinese Meteorological Administration, are shown in colors.

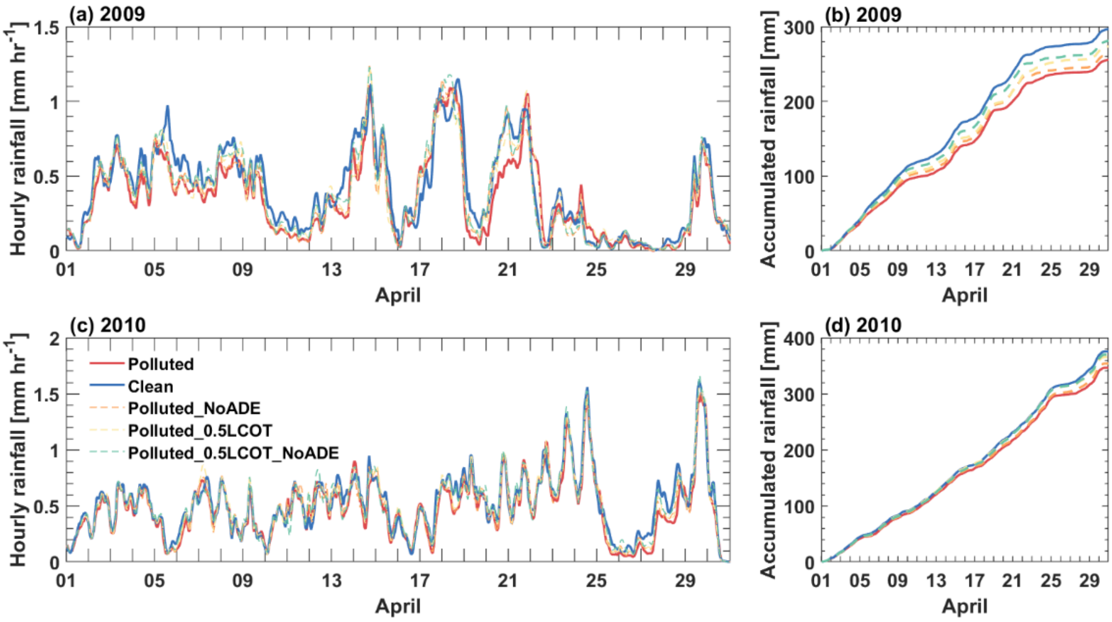

Figure S5. Time series of simulated hourly and accumulated rainfall from the sensitivity experiments of (a, b) April 2009 and (c, d) April 2010, respectively. The color legends for the sensitivity experiments are shown inset.

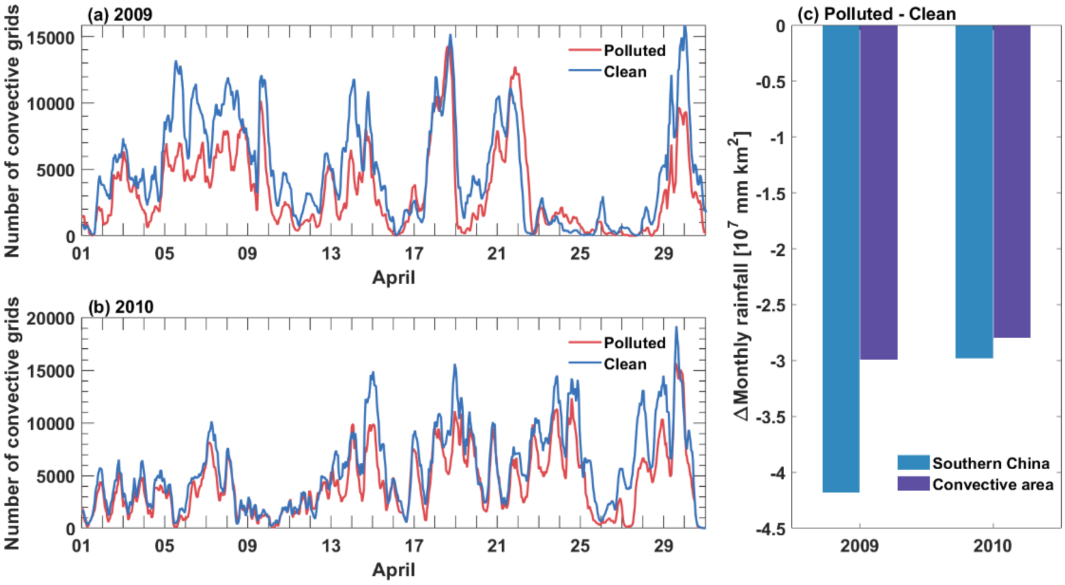

Figure S6. Time series of the simulated number of surface grids with convective rainfall, defined as surface grids with ≥35 dBZ RADAR reflectivity in the vertical column above, for (a) 2009 and (b) 2010 under polluted (red) and clean (blue) conditions. (c) The differences in monthly rainfall between the polluted simulations and the clean simulations for the entire domain of Southern China (blue bars) and for only the convective area within Southern China (purple bars).

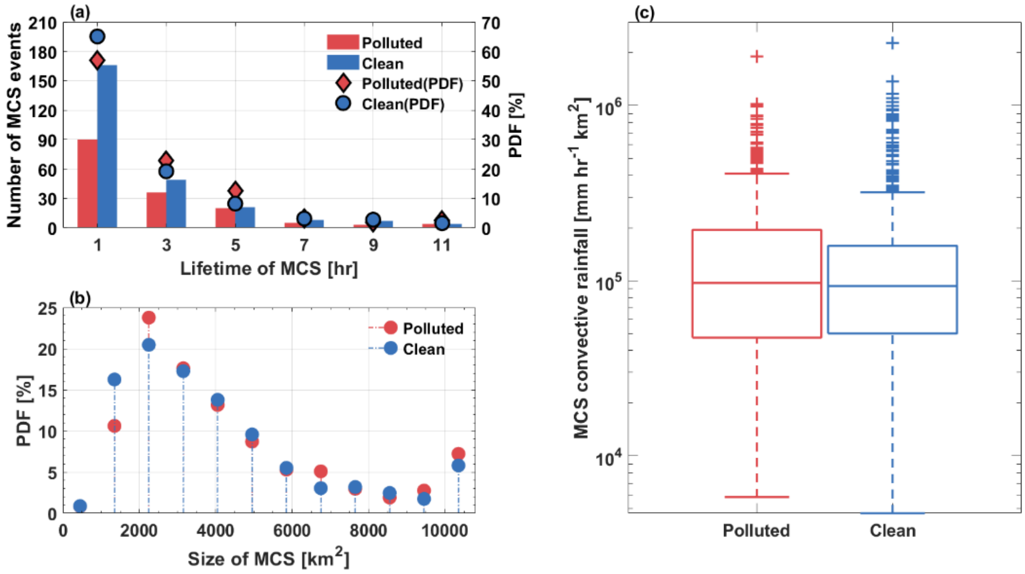

Figure S7. (a) Lifetimes of simulated MCSs. Vertical bars indicate the numbers of MCSs with specific lifetimes. Symbols indicate the probability distribution function of MCS lifetime, i.e., the number of MCSs with a specific lifetime, normalized by the total number of simulated MCSs. (b) The probability distribution function of MCS size, i.e., the number of MCSs with a specific size, normalized by the total number of simulated MCSs. (c) Box plots of the simulated MCS convective rainfall volume intensity, i.e., the hourly convective rainfall volume associated with each individual MCS. Results from the polluted and clean simulations are shown in red and blue, respectively.

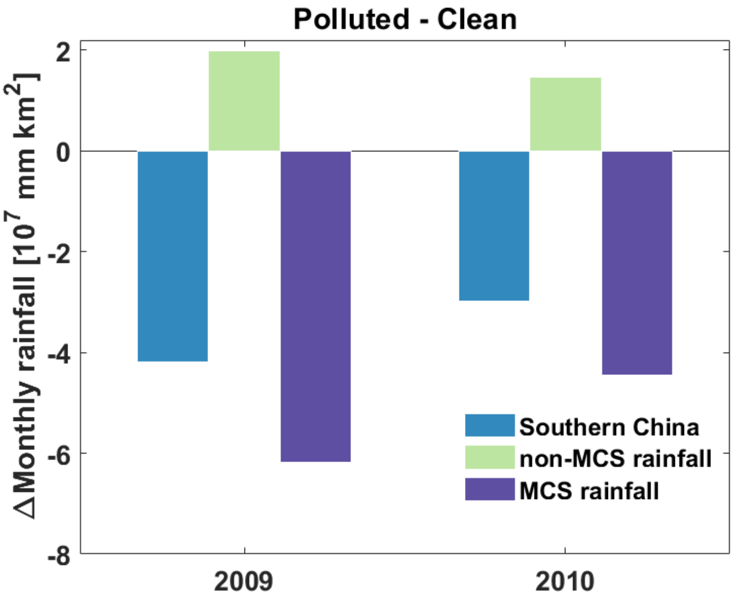

Figure S8. Differences in the monthly rainfall between the polluted simulations and clean simulations for: total rainfall over the domain of Southern China (blue bars), rainfall not associated with MCSs (‘non-MCS rainfall’, green bars), and rainfall associated with MCSs (‘MCS rainfall’, purple bars).

Table S1. Physical and chemical configurations for the WRF-Chem simulations in this study.

Physical and chemical schemes	***Options***
Gas-phase chemistry	CBMZ
Aerosol microphysics and chemistry	MADE/SORGAM
Cloud microphysics	Morrison + DeMott et al. (2010) for ice nuclei activation
Cumulus physics	Grell 3D
Shortwave radiation	Goddard
Longwave radiation	RRTM
Surface layer exchange coefficients	Monin-Obukhov
Land surface (land-atmosphere interaction)	Noah
Planetary boundary layer	Yonsei University
Biogenic emissions	MEGAN

Table S2. Diagnostics of simulated surface and atmospheric thermodynamic variables in the sensitivity simulations for April 2010. Values are averages over the land areas in the simulated Southern China domain.

	Sensitivity simulations					
	Polluted	Polluted _NoADE	Polluted _0.5 LCOT	Polluted _NoADE _0.5 LCOT	Clean	**Percent impacts of aerosols (Polluted -Clean)/Polluted**
AOD (all sky)	0.386	0.360	0.361	0.334	0.0625	+84%
LCOT	86.2	84.6	42.3	41.4	45.4	+47%
April accumulated precipitation [mm]	346	354	366	370	376	-8.5%
Downward shortwave radiation at the surface [W m^{-2}]	191	197	207	213	217	-13%
T at 2 m [ºC]	20.3	20.4	20.6	20.7	20.9	-3.1%
Convective available potential energy (CAPE) [J]	386	388	395	395	435	-13%
Cloud top temperature [ºC]	-14.7	-15.1	-15.6	-.15.8	-15.8	+6.9%
Vertical velocity [m s^{-1}]	0.0790	0.0808	0.0816	0.0831	0.0858	-8.7%
Moisture convergence [10^{-6} g cm^{-2} hPa^{-1} s^{-1}]	2.15	2.22	2.20	2.23	2.53	-18%
Precipitable water [mm]	39.5	39.5	39.6	39.7	39.8	-0.80%

Table S3. Diagnostics of the simulated microphysical variables in the sensitivity simulations for April 2009 and 2010. Unless otherwise indicated, values are averages over the land areas in the simulated Southern China domain.

Microphysical variables		***2009***		***2010***	
		Polluted	**Clean**	**Polluted**	**Clean**
Liquid cloud (below 750 hPa)	**Droplet number concentration [cm^{-3}]**	21.2	5.00	32.0	7.69
	Mixing ratio [10^{-3} g kg^{-1}]	27.5	20.0	39.5	28.5
Ice cloud (750 hPa to 100 hPa)	**Ice crystal number concentration [cm^{-3}]**	0.0150	0.0174	0.0199	0.0212
	Mixing ratio [10^{-3} g kg^{-1}]	5.46	6.57	7.26	7.88
Rain (below 500 hPa)	**Raindrop number concentration [cm^{-3}]**	0.0148	0.0293	0.0168	0.0319
	Mixing ratio [10^{-3} g kg^{-1}]	17.8	22.7	22.7	27.1
Snow and graupel (750 hPa to 100 hPa)	**Number concentration [10^{-3} cm^{-3}]**	0.744	0.837	0.917	0.938
	Mixing ratio [10^{-3} g kg^{-1}]	13.3	14.2	19.2	18.7